



Anti-Ferroptotic Effects of bone Marrow Mesenchymal Stem Cell-Derived Extracellular Vesicles Loaded with Ferrostatin-1 in Cerebral ischemia-reperfusion Injury Associate with the GPX4/COX-2 Axis

Junying Liu¹ · Yan Zhou² · Chenchen Xie³ · Ci Li⁴ · Li Ma⁵ · Yamei Zhang¹

Received: 26 March 2022 / Revised: 13 September 2022 / Accepted: 26 September 2022 / Published online: 2 November 2022
© The Author(s), under exclusive licence to Springer Science+Business Media, LLC, part of Springer Nature 2022

Abstract

Accumulating evidence of the critical role of Ferrostatin-1 (Fer-1, ferroptosis inhibitor) in cerebral ischemia has intrigued us to explore the molecular mechanistic actions of Fer-1 delivery by bone marrow mesenchymal stem cells-derived extracellular vesicles (MSCs-EVs) in cerebral ischemia-reperfusion (I/R) injury. In vivo middle cerebral artery occlusion (MCAO) in mice and in vitro oxygen-glucose deprivation/reperfusion (OGD/R) in hippocampal neurons were developed to simulate cerebral I/R injury. After Fer-1 was confirmed to be successfully delivered by MSCs-EVs to neurons, we found that MSCs-EVs loaded with Fer-1 (MSCs-EVs/Fer-1) reduced neuron apoptosis and enhanced viability, along with curtailed inflammation and ferroptosis. The regulation of Fer-1 on GPX4/COX2 axis was predicted by bioinformatics study and validated by functional experiments. The in vivo experiments further confirmed that MSCs-EVs/Fer-1 ameliorated cerebral I/R injury in mice. Furthermore, poor expression of GPX4 and high expression of COX-2 were witnessed in cerebral I/R injury models. MSCs-EVs/Fer-1 exerted its protective effects against cerebral I/R injury by upregulating GPX4 expression and inhibiting COX-2 expression. Taken together, our study indicates that MSCs-EVs/Fer-1 may be an attractive therapeutic target for the treatment of cerebral I/R injury due to its anti-ferroptotic properties.

Keywords Cerebral ischemia-reperfusion injury · Ferroptosis · Hippocampal neurons · Bone marrow mesenchymal stem cells · Extracellular vesicles · Ferrostatin-1 · Glutathione peroxidase 4 · Cyclooxygenase-2

✉ Li Ma
mary@ibt.pumc.edu.cn

✉ Yamei Zhang
zhangyamei@edu.edu.cn

¹ Key Laboratory of Clinical Genetics, Affiliated Hospital & Clinical Medical College of Chengdu University, No. 82, North Section 2, 2nd Ring Road, 610081 Chengdu, Sichuan Province, P.R. China

² Department of Radiation Protection Medicine, Faculty of Preventive Medicine, Air Force Medical University, 710032 Xi'an, P. R. China

³ Department of Neurology, Affiliated Hospital & Clinical Medical College of Chengdu University, 610081 Chengdu, P.R. China

⁴ Department of Pathology, Affiliated Hospital & Clinical Medical College of Chengdu University, 610081 Chengdu, P. R. China

⁵ Institute of Blood Transfusion, Chinese Academy of Medical Sciences, No. 76, Huacai Road, Chenghua District, 610052 Chengdu, Sichuan Province, P. R. China

Introduction

Cerebral ischemia-reperfusion (I/R) injury is one of the most severe and complicated brain diseases, characterized by high rates of mortality and disability, seriously threatening human life and health [1–3]. Cerebral I/R injury can lead to irreversible damage, especially in the hippocampus, and transient cerebral ischemia even triggers neuronal cell death in the hippocampal region [4, 5]. It is interesting to note that ferroptosis has been increasingly appreciated as a mechanism underlying the pathological process of cerebral I/R injury [6–8]. Ferroptosis is a newly discovered programmed cell death that is characterized by iron-dependent accumulation of lipid peroxidation, serving as a promising therapeutic target in ischemic stroke [9] and cerebral I/R injury [10]. Understanding the cellular and molecular events underpinning this ferroptosis is fundamental to developing therapeutic strategies of cerebral I/R injury.

Extracellular vesicles derived from mesenchymal stem cells (MSCs-EVs) have the potential as therapeutic approaches in various diseases as they can affect disease outcomes by transferring their bioactive cargoes such as DNA, proteins/peptides, mRNAs, miRNAs, lipids, and organelles to recipient cells [11, 12]. For instance, MSCs-EVs carrying mRNAs and miRNA exhibit great performances for the therapy of I/R injuries, such as liver I/R injury and myocardial I/R injury [13, 14]. Although emerging evidence has revealed the protective role of MSCs-EVs against ferroptosis and the induced diseases [15, 16], evidence is limited on the effects of MSCs-EVs carrying Ferrostatin-1 (Fer-1) on cerebral I/R injury, which becomes the focus of the current study.

Fer-1, a ferroptosis inhibitor, is an antioxidant small molecule compound containing arylalkylamines and a potent inhibitor of ferroptosis [17]. Of note, Fer-1 has been reported to relieve the neuroinflammation induced by lipopolysaccharides [18]. In addition, Fer-1 treatment reverses SSAT1 upregulation-induced ferroptosis and viability loss in tertbutyl-hydroksyperoxide-exposed neurons, thus alleviating cerebral I/R injury [19]. More importantly, Fer-1 treatment can upregulate expression of glutathione peroxidase 4 (GPX4) after subarachnoid hemorrhage [20]. GPX4 can affect ferroptosis, the inactivation of which worsens renal I/R injury by causing production of reactive oxygen species (ROS) [21]. Moreover, GPX4 can inhibit cerebral I/R-induced inflammation in a rat model of cerebral artery occlusion by inhibiting cyclooxygenase-2 (COX-2) [22, 23]. Abnormally expressed COX-2 has also been detected in cerebral I/R injury, and the reduction of COX-2 expression can ameliorate the brain injury [24].

Motivated by the above-mentioned evidence, we propose the hypothesis that MSC-EVs can act as a drug carrier to facilitate the treatment of cerebral I/R injury. In this study, we loaded Fer-1 into MSCs-EVs (MSCs-EVs/Fer-1) and performed a series of experiments *in vitro* and *in vivo*, with the purpose to validate the effects of MSCs-EVs/Fer-1 and the underlying molecular mechanism on ferroptosis, hippocampal neuronal injury, and ultimately the cerebral I/R injury.

Materials and Methods

Ethics Statement

The experimental procedure and animal use protocols were approved by the Animal Ethics Committee of the Affiliated Hospital of Chengdu University. Mice used for *in vivo* studies were cared for in accordance with the *Guide for the*

Care and Use of Laboratory Animals published by the US National Institutes of Health [25].

Bioinformatics Analysis

Inhibitors of ferroptosis were obtained through the ferroptosis data FerrDb. Genes related to inhibitors of ferroptosis were retrieved through CTD database. Gene expression microarray GSE104462 (control sample=3; Fer-1-treated sample=3) before and after treatment with Fer-1, was obtained through GEO database. The mouse cerebral I/R-related microarray GSE23160 (sham operation sample=8; I/R sample=24) was downloaded. The R language “limma” package was used to screen the differentially expressed genes (DEGs) with p value < 0.05 as the threshold.

Isolation and Identification of MSCs-EVs

Mouse bone marrow MSCs (MUBMX-01001, Cyagen, Suzhou, China) were cultured in bone marrow MSC complete medium (MUBMX-90,011, Cyagen). When reaching 80–90% confluence, the cells were rinsed three times with phosphate buffer saline (PBS) and then transferred to EV-depleted and serum-free Dulbecco’s modified Eagle’s medium (DMEM). After 48 h, the supernatant was harvested to isolate EVs using an ultracentrifugation-based method (Optima XPN-100, Beckman) [26].

The cellular EVs were characterized for morphology by transmission electron microscope (TEM; TECNAI G2 20 S-TWIN, FEI) [27], for particle size by nanoparticle tracking analysis (NTA) using a nanoparticle trafficking analyzer (NanoSight LM10, malvernpanalytical) [28], and for EV surface marker proteins by Western blot using the following antibodies (Abcam Inc., Cambridge, UK): rabbit anti-CD63 (ab216130, 1:2000), rabbit anti-CD9 (ab223052, 1:500), rabbit anti CD81 (ab109201, 1:1000), and rabbit anti-calnexin (ab227310, 1:1000).

Characterization of Loading of Fer-1 and Uptake of EVs *in vitro*

Proteins from EVs were diluted with PBS, which were mixed thoroughly with an equal amount of Fer-1 solution (SML0583-5 mg, Sigma). The EVs encapsulated with Fer-1 were thus obtained. The standard Fer-1 was diluted with dimethyl sulfoxide (DMSO) into a series of concentration gradient standard solutions (2, 5, 10, 20, 30, 40, 50 $\mu\text{g}/\text{mL}$), and the standard curve of Fer-1 was plotted to calculate its regression equation and correlation coefficient. According to the regression equation, the concentration and encapsulation rate of Fer-1 in EVs were measured by high-performance liquid chromatography (HPLC). The entrapment efficiency

(EE) was calculated as follows: $EE (\%) = [(amount\ of\ drug\ delivery - amount\ of\ free\ Fer-1\ in\ the\ system) / amount\ of\ drug\ delivery] \times 100\%$.

MSCs-EVs with Fer-1 were labeled with red fluorescent dye Dil (C1036, Beyotime) according to the instructions. Specifically, 5 μ L of PKH-67 working solution (MINI67, Sigma) was co-incubated with cells at 37 °C for 24 h. After nucleus staining with DAPI, fluorescence changes were imaged with a confocal microscope (AX/AXR, Nikon, Japan).

Characterization of Uptake of MSCs-EVs/Fer-1 *in vivo*

MSCs-EVs/Fer-1 were labeled using Dil (red), and then injected into middle cerebral artery occlusion (MCAO) mice via tail vein. The cerebral cortex tissues were fixed and sectioned. The nuclei were stained with DAPI, while hippocampal neurons were labeled with neuron-specific enolase (NSE; ab180943, 1 : 50, Abcam). After 1 h-incubation with secondary antibody, sections were mounted and photographed using a confocal fluorescence microscope (AF6000, Leica), with results analyzed with Image J software.

In vitro Release Rate Measurement

The *in vitro* drug release of MSCs-EVs/Fer-1 was studied using a dynamic dialysis method with PBS as the release medium [29]. Briefly, equal amounts of Fer-1 and MSCs-EVs/Fer-1 were placed in dialysis bags (MW=10,000) containing 4 mL of release medium. The dialysate was collected after shaking at 100 rpm, 37 °C, and the amount of drug released was recorded. Meanwhile, 1 mL of the solution was replaced with an equal volume of fresh PBS. The amount of Fer-1 released from free Fer-1 and MSCs-EVs/Fer-1 was analyzed using HPLC (Agilent 1290, Agilent).

Culture of Primary Cortical Hippocampal Neurons

Mouse primary hippocampal neurons were isolated from neonatal C57BL/6 mice (Dashuo Laboratory Animal Technology Co. Chengdu, China). Mice were decapitated under aseptic conditions to isolate the cerebral cortex. The cerebral cortex tissues were minced, and digested in 0.125% trypsin for 30 min, which was halted by DMEM/F12 medium (A4192001, Gibco) with FBS (10,099,141, Thermo Fisher Scientific). The cell suspension was filtered and centrifuged (at 3,000 g for 10 min), and the cell pellet was resuspended in DMEM/F12 and incubated at 37 °C, 5% CO₂. The cell culture continued the next day in serum-free medium, and agranulocyte (5 μ g/mL, 147-94-4, Sigma) was added to the medium to prevent the growth of non-hippocampal neurons.

After 24 h, the normal medium was used, and the medium was renewed every 72 h thereafter. *In vitro* culture was performed for 7–21 days for experiments.

Immunofluorescence Identification of Cortical Hippocampal Neurons

Cortical hippocampal neurons were seeded in a cell culture plate containing slides at a density of 70–80%, with the slides removed after cell adherence to the wall. Cells were then fixed with 4% paraformaldehyde, permeabilized with 0.3% Trion X-100, and blocked with 10% serum containing 1% bovine serum albumin (BSA) and 0.3% Trion X-100. Next, the cells were incubated with primary antibodies (Abcam) against rabbit monoclonal antibody to NSE (ab180943, 1:50) and mouse monoclonal antibody to glial fibrillary acidic protein (GFAP; ab279290, 1:1000) overnight at 4 °C, followed by incubation for 1 h at 37 °C with secondary antibody the next day. Images were observed under a fluorescence microscope (IX73, Olympus), with NSE showing green fluorescence and GFAP showing red fluorescence.

Cell Transduction and Grouping

HEK293 FT cells (Thermo Fisher Scientific, R70007) were transfected with a mixture containing three plasmids and 25 kDa linear polyethyleneimine (PEI; Polysciences, Inc., 23966-100) to generate high-titer lentivirus. Particles containing lentiviral particles were resuspended in ice-cold PBS (Thermo Fisher Scientific, 10,010,023; pH 7.4), divided into 10 μ L aliquot and stored at –80 °C. Hippocampal neurons were transduced with lentivirus (titer of 1×10^9 TU/mL) carrying oe-NC (multiplicity of infection [MOI] of 10), oe-COX-2 (MOI of 10), sh-NC (MOI of 15) and sh-GPX4 (MOI of 15). The silencing sequences are shown in Supplementary Table 1.

Development of Oxygen-Glucose Deprivation/Reperfusion (OGD/R)-Induced Cell Model

Hippocampal neurons were exposed to OGD/R. After the hippocampal neurons were cultured and matured, the medium was renewed with serum-free DMEM and the cells were cultured for 2 h at 37 °C in 5% CO₂ and 95% N₂ (OGD). Then the medium was replaced by normal medium and the cells continued to culture in 5% CO₂ and 95% O₂ for 24 h.

MTT Assay

Cells were seeded in 96-well plates containing 0.5% fetal bovine serum (FBS) at a density of 5×10^3 cells/well. Cell viability was measured by MTT after 24 h. Cells were incubated with MTT solution (0.5 mg/mL) at 37 °C for 3 h. The formazan was dissolved in DMSO. Absorbance at 570 nm was measured using a microplate reader (Scientific Varioskan LUX, Thermo Fisher Scientific).

Detection of Intracellular Iron Content

Total iron in cell lysates was quantified using an iron assay kit (ab83366, Abcam). Cells were lysed in 4 times the volume of iron assay buffer and centrifuged at 16,000 g for 10 min to remove insoluble material. The iron reducing agent (5 μ L) was added to 50 μ L of sample for total iron determination. Next, 100 μ L of iron probe solution was added to the samples and incubated for 60 min at 4 °C without light exposure. Absorbance at 593 nm was assessed by a microplate reader (Scientific Varioskan LUX, Thermo Fisher Scientific).

Flow Cytometric Apoptosis Assay

Apoptosis of hippocampal neurons was detected using Annexin V-fluorescein isothiocyanate (FITC)/propidium iodide (PI) kit (C1062L, Beyotime). Cells were seeded in 6-well plates at a density of 1×10^6 cells per well. Cells were resuspended in 195 μ L Annexin V-FITC conjugate, followed by incubation with 5 μ L Annexin V/FITC and 10 μ L PI for 15 min at room temperature in the dark. Flow cytometry was performed within 20 min.

ROS Detection

ROS assay kit (S0033S, Beyotime) was used as described in instructions [30]. Cerebral cortex tissues were homogenized and then centrifuged to collect the supernatant. Then, a fluorescent probe of DCFH-DA was added to the supernatant (190 μ L) and incubated in the dark for 30 min at 37 °C. An automated fluorescent microplate reader (Scientific Varioskan LUX, Thermo Fisher Scientific) was used to quantify the green fluorescence intensity.

Hippocampal neurons were seeded into 6-well plates, and DCFH-DA was diluted with serum-free medium. Diluted DCFH-DA was incubated for 20 min at 37 °C. Fluorescence intensity was detected using a fluorescent microplate reader.

Detection of Glutathione (GSH) and Malondialdehyde (MDA) Production and Tumor Necrosis Factor- α (TNF- α) and Interleukin-1 β (IL-1 β) Levels

Mouse cerebral cortex tissues were homogenized and centrifuged (4,000 r/min) at 4 °C, for 10 min to collect supernatant, which was stored at -20 °C. The cells were seeded in 6-well plates, centrifuged and collected. The production of GSH was determined using GSH kit (A006-2-1, Jiancheng Biotech, Nanjing, China). Briefly, 0.5 mL of the sample to be tested was drawn, mixed with 2 mL of the reagent-application solution and centrifuged at 3500–4000 rpm for 10 min. Next, 1 mL of the supernatant was collected and mixed with sample and reagent, left to stand for 5 min and developed. The absorbance value was measured at a wavelength of 420 nm [31]. Mouse cerebral cortex tissues or cultured neurons were collected as described above and the production of MDA was determined using MDA kit (thio-barbituric acid [TBA] method; A003-1-2, Jiancheng Biotech). This method measures the color produced during the reaction of TBA with MDA by spectrophotometry. Briefly, PBS-washed cells were collected and lysed with the lysis buffer provided with the kit to prepare a supernatant. The supernatant was reacted with 200 μ L of the malondialdehyde reaction solution at 100 °C for 15 min, and a microplate reader was used to measure the production of MDA at 532 nm [31].

In addition, we determined the levels of TNF- α (H052-1, Nanjing Jiancheng Institute of Biological Engineering, Jiangsu, China) and IL-1 β (H002, Nanjing Jiancheng Institute of Biological Engineering, Jiangsu, China) by enzyme-linked immunosorbent assay according to the kit instructions [32]. After collecting mouse cerebral cortex tissue or cultured neurons, RIPA reagent (P0013C, Beyotime, Shanghai, China) was added to homogenize or lyse the tissue or cells. Next, tissue homogenates or cell lysates were collected for ELISA detection. Tissue homogenates or cell lysates were added to TNF- α and IL-1 β antibody-coated plates and incubated for 2 h at room temperature. The solution was then removed and incubated with biotinylated goat anti-rabbit IgG (h+L) antibody for 45 min at 37 °C. Next, it was washed three times with PBS and incubated with enzyme-labeled Streptavidin antibody for 30 min at 37 °C. Finally, TMB solution was added and incubated at room temperature for 20 min. The OD values of the wells were measured at a wavelength of 490 nm using a microplate reader (Bio-Tek, Winooski, VT, USA). The BCA method (P0012, Beyotime, Shanghai, China) was used. According to the protein concentration in tissue homogenate or cell lysate, the content of TNF- α and IL-1 β in tissue or cells per mg protein was calculated.

RNA Isolation and Quantification

Total RNA was isolated from hippocampal neurons and cerebral cortex tissues with TRIzol reagent (10,296,010, Thermo Fisher Scientific), followed by RNA quantification with Nanodrop (Nanodrop 2000, Thermo Fisher Scientific). Total RNA (1 μ g) was reverse transcribed using TaqMan reverse transcription reagent (N8080234, Thermo Fisher Scientific). PCR analysis was performed using the PowerUp SYBR Green Premix Kit (A25741, Thermo Fisher Scientific). The fold changes were calculated using $2^{-\Delta\Delta C_t}$. The primer sequences are shown in Supplementary Table 2.

Western Blot

Total protein was extracted from cells and cerebral cortex tissues using radio-immunoprecipitation assay (RIPA) lysis buffer (P0013B, Beyotime) containing 4% protease inhibitor (P1005, Beyotime). Protein concentration was determined using the BCA Protein Assay Kit (23,227, Thermo Fisher Scientific). After sodium dodecyl sulfate-polyacrylamide gel electrophoresis (SDS-PAGE), separated proteins were transferred to polyvinylidene fluoride (PVDF) membranes (FFP24, Beyotime) by wet transfer method. The membranes were blocked with Tris-buffered saline with 0.1% (v/v) Tween 20 (TBST) containing 5% skim milk (P0216-300 g, Beyotime). Membranes were probed with primary antibodies (Abcam) at 4 °C overnight: rabbit anti-CD9 (ab223052, 1:1000), rabbit monoclonal anti-CD81 (ab109201, 1:1000), rabbit monoclonal anti-CD63 (ab217345 1:1000), rabbit anti-cleaved caspase 3 (ab2302, 1:500), rabbit anti-caspase 3 (ab184787, 1: 1000), rabbit monoclonal anti-B-cell lymphoma 2 (Bcl-2; ab182858, 1:2000), rabbit monoclonal anti-Bcl-2-associated X protein (Bax; ab32503,1:1000), rabbit anti-COX-2 (MA5-14568, 1:1000, Invitrogen), rabbit monoclonal anti-GPX4 (ab125066, 1:500), and rabbit monoclonal anti-glyceraldehyde-3-phosphate dehydrogenase (GAPDH; ab181602, 1:10,000). After TBST washing, the membranes were incubated with horseradish peroxidase (HRP)-labeled secondary antibody goat anti-rabbit (A0208, Beyotime) at room temperature for 1 h. The immunocomplexes on the membrane were visualized via enhanced chemiluminescence (ECL) reagent (WP20005, Thermo Fisher Scientific) using ECL detection system (ChemiDoc XRS+, Bio-Rad). Proteins were quantified using ImageJ software, with GAPDH as an internal reference.

Development of MCAO Mouse Models

Male C57BL/6 mice (8-week-old; 21–23 g; Dashuo Laboratory Animal Technology Co. Chengdu, China) were housed in separate cages (temperature: 22–25 °C, humidity:

60–65%) in a specific pathogen free laboratory. The mice were acclimatized for one week to observe their status.

Cerebral ischemia was induced by occlusion of the middle cerebral artery occlusion. C57BL/6 mice were anesthetized by 1% pentobarbital sodium (40 mg/kg) intraperitoneally and fixed on the operating table. The neck was exposed and disinfected, and an incision was made in the midline of the neck, and the skin, muscle and subcutaneous tissues were sequentially and bluntly separated. The main trunk of the right common carotid artery, external, and internal carotid artery were fully exposed. The right common carotid artery was ligated at the proximal using an 8–0 thread, and the external carotid artery was ligated at the distal end. A small incision was made at the distal end of the external carotid artery, and the 6–0 thread was inserted into the external carotid artery and then the internal carotid artery, and the insertion was stopped when a sense of resistance to insertion was felt, at which point the length of the inserted tethered wire was approximately 8–9 mm. After the insertion was completed, the wire was left in place for 1 h. The body temperature of the mice was maintained during this time. Finally, the tethered wire was removed and reperfused, and the incision was sutured.

In the sham-operation, the nylon thread was inserted only into the external carotid artery, which could not block the blood flow, and the rest of the steps were the same as in the MCAO modeling.

Lentiviruses containing COX-2 overexpression vector (oe-COX-2), short hairpin RNA against GPX4 (sh-GPX4), or the negative controls (sh-NC and oe-NC) were injected into the lateral ventricles of mice (40 μ L) before reperfusion. Fer-1 and MSCs-EVs/Fer-1 were administered by tail vein injection (100 μ g/g) 30 min after reperfusion, and mice were sacrificed after four consecutive days of administration. There were 10 mice in each group. The silencing sequences are shown in Supplementary Table 3.

Neurological Deficit Scores

Mice were subjected to neurological deficit scores after being awoken from anesthesia. The mice were scored blindly for neurological deficits 24 h after perfusion. Specifically, no neurological deficits (showing normal and spontaneous movements) scored 0; mild focal neurological deficits (not fully extended contralateral forelimb) scored 1; moderate focal neurological deficits (repetitive rotation to the contralateral side) scored 2; severe focal neurological deficits (descending to the contralateral side) scored 3; and the depressed state or death (being unable to walk autonomously and consciously) scored 4.

Morris Water Maze (MWM) test

The MWM test was utilized as previously described [33, 34] to assess learning and memory abilities of animals after MCAO. A Morris pool (diameter of 120 cm and 50 cm) was filled with water to 40 cm and divided into 4 quadrants. A black station (6 cm diameter, 28 cm high, 2 cm below water) was placed in the first quadrant for the mice to position the platform. The titanium dioxide was added to the water, which was stirred well to make the water turbid and limit the normal visible field of view from the mice. The water temperature was adjusted to 19–22 °C. A video camera was placed above the platform and connected to a computer to facilitate data collection. Mice were first acclimatized and placed in quadrants I–IV in order one day in advance. When a test was completed, the mice were removed from the water in time and dried.

Mice after modeling were subjected to the spatial navigation test and their escape latency was recorded. The mice entered the water from four quadrants in turn, and the test time for each quadrant was 60 s. If the mouse could climb to the platform within the specified time and stay for more than 3 s, they were considered to have successfully found the platform. The time spent by the mice to find the platform was recorded, and the determined escape latency was the average of that of mice spent in the 4 quadrants. The test period was 5 days. Longer escape latency reflected worse spatial learning ability of the mice.

At the end of the escape latency experiment, the station hidden under the water surface was removed. It was placed in the water for 90 s according to the above-mentioned four quadrant entry points, and the number of times the mice crossed the original platform quadrant within 90 s was tested.

Assessment of Brain Edema

Cerebral cortex tissues were collected immediately 24 h after MCAO, and wet tissues were weighed. Subsequently, the cerebral cortex tissue samples were dried in an oven at 95 °C for 48 h and weighed again (as dry weight). Brain water content was calculated as $[(\text{wet tissue weight} - \text{dry tissue weight})/\text{wet tissue weight}] \times 100\%$.

Prussian Blue Staining

Paraffin-embedded sections of cerebral cortex tissues were dewaxed and incubated with Perl's reaction solution (6% potassium ferricyanide solution and 10% hydrochloric acid 1:1, ready to use; about 0.6–0.8 mL per section) at room temperature for 9 h. Afterwards, sections were incubated with nuclear solid red staining solution (C0151, Beyotime)

at room temperature. Thereafter, the sections were mounted and observed under a microscope. The area of blue iron precipitation was measured with the Image-Pro 6.0 software.

TTC Staining

After 24 h of perfusion, the mice were euthanized under anesthesia. Then, the brain was quickly removed, freshly dissected into coronal sections ($n=10$). Subsequently, the sections were stained with 2% TTC solution (T8877, Sigma) for 15 min at 37 °C in the dark, with white infarcted and red non-infarcted areas visible in the cerebral cortex tissues. Brain infarct area was calculated using ImageJ image software (ImageJ 1.42, Wayne Rasband, National Institutes of Health) [35].

Nissl Staining

Mouse cerebral cortex tissues were fixed in 4% paraformaldehyde for 48 h, dehydrated, embedded in paraffin and prepared into sections for Nissl staining according to the instructions of Nissl staining kit (C0117, Beyotime). The sections were stained with Nissl staining solution for 3–10 min, washed twice with distilled water, rehydrated in 95% and 70% ethanol, permeabilized and mounted. Finally, sections were observed under a microscope, where the tissues were shown in blue-purple.

TUNEL Staining

Apoptosis assay was performed using TUNEL Apoptosis Detection Kit (C1086, Beyotime). Paraffin-embedded brain sections were treated with 20 $\mu\text{g}/\text{mL}$ of proteinase K without Dnase for 15 min at 20 °C and incubated with 3% hydrogen peroxide solution at room temperature for 20 min. The sections were incubated with the prepared TUNEL solution (one sample was mixed with 5 μL of TdT enzyme, 45 μL of fluorescence labeling solution and 50 μL of TUNEL detection solution, and then added to the sample) for 60 min at 37 °C without light exposure and sealed with fluorescence decay resistant medium before observation under a fluorescence microscope.

Statistical Analysis

All data were analyzed using SPSS 21.0 statistical software (IBM, Armonk, NY). Measurement data were expressed as mean \pm standard deviation. Unpaired *t*-test was applied for comparison between two groups, and one-way analysis of variance (ANOVA) was conducted for comparison among multiple groups. Statistical analysis in relation to time-based measurements within each group was realized using

repeated measures ANOVA. Statistical significance was set at $p < 0.05$.

Results

MSCs-EVs Deliver Fer-1 into Hippocampal Neurons

To investigate the effect of MSCs-EVs on cerebral I/R injury by delivering Fer-1, we first isolated EVs from MSCs, and the results of TEM and NTA showed that EVs had a spherical structure (Supplementary Fig. 1 A) with a diameter mainly distributed at 126.5 nm (Supplementary Fig. 1B). Also, EVs significantly expressed CD9, CD81, and CD63, but did not express Calnexin (Supplementary Fig. 1 C).

Next, we verified whether MSCs-EVs delivered Fer-1 into hippocampal neurons. After isolation of mouse primary cortical hippocampal neurons, we observed NSE-labeled hippocampal neurons and found that hippocampal neurons had plump cytosomes and more protrusions growth, while no GFAP-labeled glial cells were found (Supplementary Fig. 1D). Then we loaded Fer-1 on MSCs-EVs using ultrasonic incubation method and detected Fer-1 in EVs by HPLC method. MSCs-EVs/Fer-1 were with the same retention time as Fer-1 standards, which indicated that Fer-1 was successfully loaded on MSCs-EVs. Moreover, the average EE of MSCs-EVs on Fer-1 was 23.07%. Then, hippocampal neurons were incubated with Dil and PKH-67-labeled EVs for 24 h. A clear fluorescence distribution was found in hippocampal neurons under a fluorescence microscope, and this result indicated that MSCs-EVs/Fer-1 could be effectively internalized by hippocampal neurons (Fig. 1A).

To investigate whether MSCs-EVs carried Fer-1 into the brain of MCAO mice and thus exerted therapeutic effects, we injected Dil-labeled MSCs-EVs/Fer-1 into MCAO mice through the tail vein, and the results are shown in Fig. 1B. Clear green fluorescence and red fluorescence can be observed in the ischemic lesion area, and this result confirmed that EVs were present in hippocampal neurons in vitro, while MSCs-EVs/Fer-1 could be well taken up by MCAO mice.

In vitro release rate assay could predict the in vivo kinetics of the drug after administration. The Fig. 1C showed the cumulative release rates of Fer-1 and MSCs-EVs/Fer-1 over time. Free Fer-1 was released in large quantities after 10 h, accompanied by relatively high cumulative release rate and greatly changed slope of the release rate curve. However, the release amount changed little in 20–50 h, and the cumulative release rate did not change much. The slope of the release rate curve was relatively small. Additionally, MSCs-EVs/Fer-1 showed a slow release, slowly increased release amount, and a sustained increase in the cumulative release

rate. The slope of the release rate curve was larger than that of free Fer-1 in the same period. The above results show that Fer-1 has some slow-release properties after being loaded into EVs.

The above results indicate the successful isolation of MSCs-EVs. In addition, MSCs-EVs can deliver Fer-1 into hippocampal neurons, achieving a slow-release effect.

MSCs-EVs/Fer-1 Protect Against OGD/R-Induced Hippocampal Neuronal Damage

Next, we explored the effect of MSCs-EVs/Fer-1 on cerebral I/R injury in vitro. An OGD/R-induced cell model was first constructed, and the intracellular iron was accumulated. However, in the OGD/R-exposed cells treated with Fer-1, iron was less accumulated, and the iron accumulation was distinctly reduced in the OGD/R-exposed cells treated with MSCs-EVs/Fer-1 (Supplementary Fig. 2A).

The results of MTT assay and flow cytometry showed that OGD/R-exposed cells showed curtailed cell viability but increased cell apoptosis. In OGD/R-exposed cells treated with Fer-1 or MSCs-EVs/Fer-1, cell viability was enhanced while cell apoptosis was decreased (Supplementary Fig. 2B-C).

Meanwhile, in the OGD/R-exposed cells, ratio of cleaved caspase 3/caspase 3 and protein expression of Bax were increased, accompanied by diminished Bcl-2 protein level. On the contrary, in the OGD/R-exposed cells treated with Fer-1, the ratio of cleaved caspase 3/caspase 3 and protein level Bax was reduced, accompanied by elevated Bcl-2 expression. These changes were much more notable in the OGD/R-exposed cells treated with MSCs-EVs/Fer-1 (Supplementary Fig. 2D).

ROS and MDA production was increased and GSH production was decreased in the OGD/R-exposed cells. However, in the supernatant of OGD/R-exposed cells treated with Fer-1 or MSCs-EVs/Fer-1, the ROS and MDA production was decreased and GSH production was increased (Supplementary Fig. 2E-G). Additionally, inflammatory factors (TNF- α , IL-1 β , and prostaglandin E2 [PGE2]) were increased in the supernatant of the OGD/R-exposed cells, while opposite results were found in the supernatant of OGD/R-exposed cells treated with Fer-1 or MSCs-EVs/Fer-1 (Supplementary Fig. 2H).

Together, MSCs-EVs/Fer-1 could inhibit the accumulation of iron, increase cell viability, and reduce apoptosis in OGD/R-exposed hippocampal neurons.

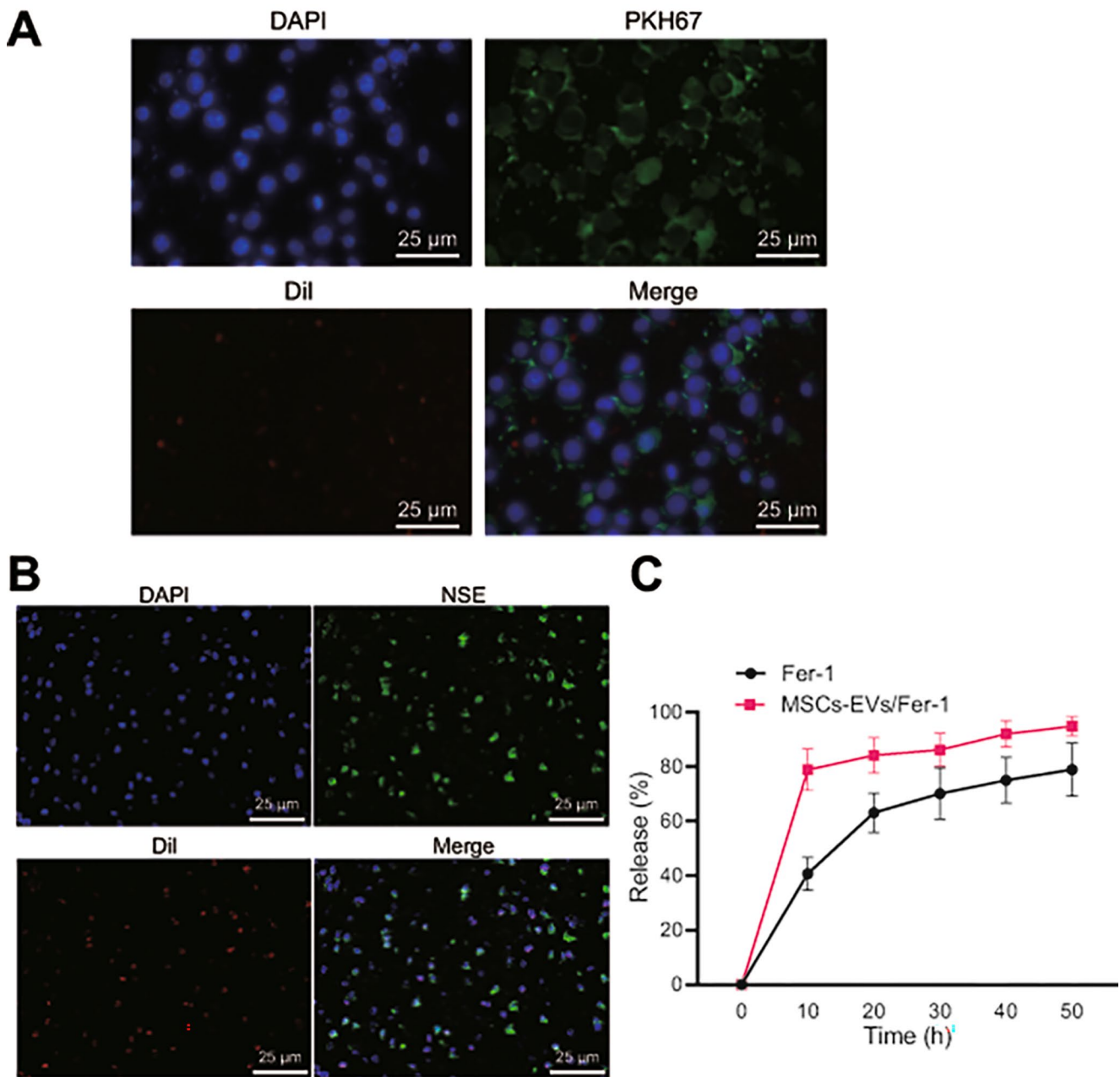


Fig. 1 MSCs-EVs/Fer-1 can be delivered to hippocampal neurons. **A**, Confocal microscopy observation of EVs uptake by hippocampal neurons. Blue: DAPI-labeled the nucleus; green: PKH-67-labeled EVs; red: Dil-labeled MSCs-EVs/Fer-1. **B**, Immunofluorescence

observation of MSCs-EVs/Fer-1 uptake in the ischemic lesion area of mice (n = 5). Green: NSE labeled hippocampal neurons. **C**, In vitro release rate of Fer-1 and MSCs-EVs/Fer-1. All cell experiments were repeated 3 times

MSCs-EVs/Fer-1 Ameliorate Cerebral I/R Injury by Inhibiting Ferroptosis in MCAO Mice

To further investigate the effect of MSCs-EVs/Fer-1 on cerebral I/R injury in vivo, we established the MCAO mice and injected them with MSCs-EVs/Fer-1 in the tail vein. The neurological deficit scores of MCAO mice were significantly higher compared to the sham-operated mice. However, the

neurological deficit scores of MCAO mice injected with Fer-1 or MSCs-EVs/Fer-1 were lower (Fig. 2A).

Also, MCAO mice showed longer escape latency and reduced times of crossing the quadrant with platform. Yet the opposite results were observed in the MCAO mice injected with Fer-1 or MSCs-EVs/Fer-1 (Fig. 2B-C). TTC staining results showed that the area of cerebral infarction was increased in the MCAO mice, yet MCAO mice injected

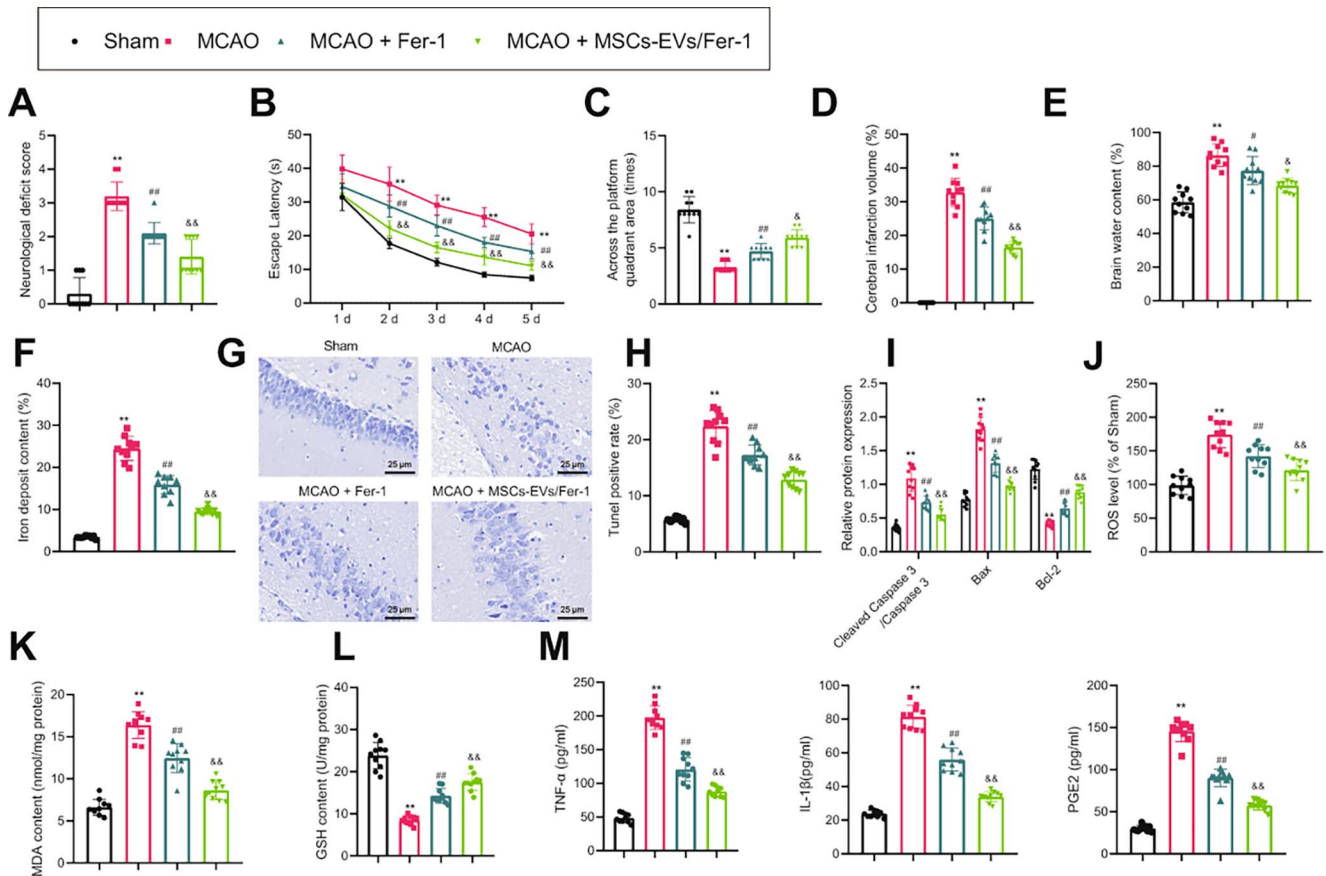


Fig. 2 Effect of MSCs-EVs/Fer-1 on cerebral I/R injury in MCAO mice. **A**, Neurological deficit scores in MCAO mice in response to Fer-1 or MSCs-EVs/Fer-1. **B**, Escape latency in MCAO mice in response to Fer-1 or MSCs-EVs/Fer-1. **C**, Number of times crossing the quadrant where the platform is located in MCAO mice in response to Fer-1 or MSCs-EVs/Fer-1. **D**, Brain infarct area analyzed by TTC staining in MCAO mice in response to Fer-1 or MSCs-EVs/Fer-1. **E**, Detection of brain water content in MCAO mice in response to Fer-1 or MSCs-EVs/Fer-1. **F**, Prussian blue staining of cerebral cortex tissues of MCAO mice in response to Fer-1 or MSCs-EVs/Fer-1. **G**, Hippocampal neuronal damage in MCAO mice in response to

Fer-1 or MSCs-EVs/Fer-1 measured by Nissl staining. **H**, Cell apoptosis in cerebral cortex tissues of MCAO mice in response to Fer-1 or MSCs-EVs/Fer-1 measured by TUNEL staining. **I**, Western blot of apoptosis-related proteins in the cerebral cortex tissues of MCAO mice in response to Fer-1 or MSCs-EVs/Fer-1. **J–L**, Detection of ROS (**J**), MDA (**K**), and GSH (**L**) production in cerebral cortex tissues in MCAO mice in response to Fer-1 or MSCs-EVs/Fer-1. **M**, Detection of inflammatory factor levels in the cerebral cortex tissues by ELISA in MCAO mice in response to Fer-1 or MSCs-EVs/Fer-1. ** $p < 0.01$ compared with the sham group; # $p < 0.05$, ## $p < 0.01$ compared with MCAO group; & $p < 0.05$, && $p < 0.01$ compared with MCAO + Fer-1 group. $n = 10$ mice for each group

with Fer-1 or MSCs-EVs/Fer-1 showed decreased area of cerebral infarction (Fig. 2D).

Furthermore, water content of cerebral cortex tissues was increased in the MCAO mice. However, the water content of cerebral cortex tissue was, in contrast, decreased in the MCAO mice injected with Fer-1 or MSCs-EVs/Fer-1 (Fig. 2E). Prussian blue staining results showed that very little iron deposition was found in the cerebral cortex tissues of few sham-operated mice, but iron deposition was accumulated in the MCAO mice. Iron content was lower in the MCAO mice injected with Fer-1 or MSCs-EVs/Fer-1 (Fig. 2F).

The hippocampal neurons of the MCAO mice lost their original structure, showed nuclear consolidation, and the number of intact hippocampal neurons was significantly

reduced. However, the number of intact hippocampal neurons in the MCAO mice injected with Fer-1 or MSCs-EVs/Fer-1 was increased (Fig. 2G). As TUNEL staining revealed, apoptosis of cells was increased in cerebral cortical tissues of MCAO mice, but decreased in the presence of Fer-1 or MSCs-EVs/Fer-1 (Fig. 2H). The ratio of cleaved caspase 3/caspase 3 and Bax protein expression was elevated, while Bcl-2 protein expression was reduced in the cerebral cortical tissues of MCAO mice, the results of which went opposite in the presence of Fer-1 or MSCs-EVs/Fer-1 (Fig. 2I).

Also, ROS and MDA production was enhanced in the cerebral cortex tissues of MCAO mice, but reduced in the MCAO mice injected with Fer-1 or MSCs-EVs/Fer-1, while GSH production was reduced in the cerebral cortex tissues of the MCAO mice but elevated in the MCAO mice

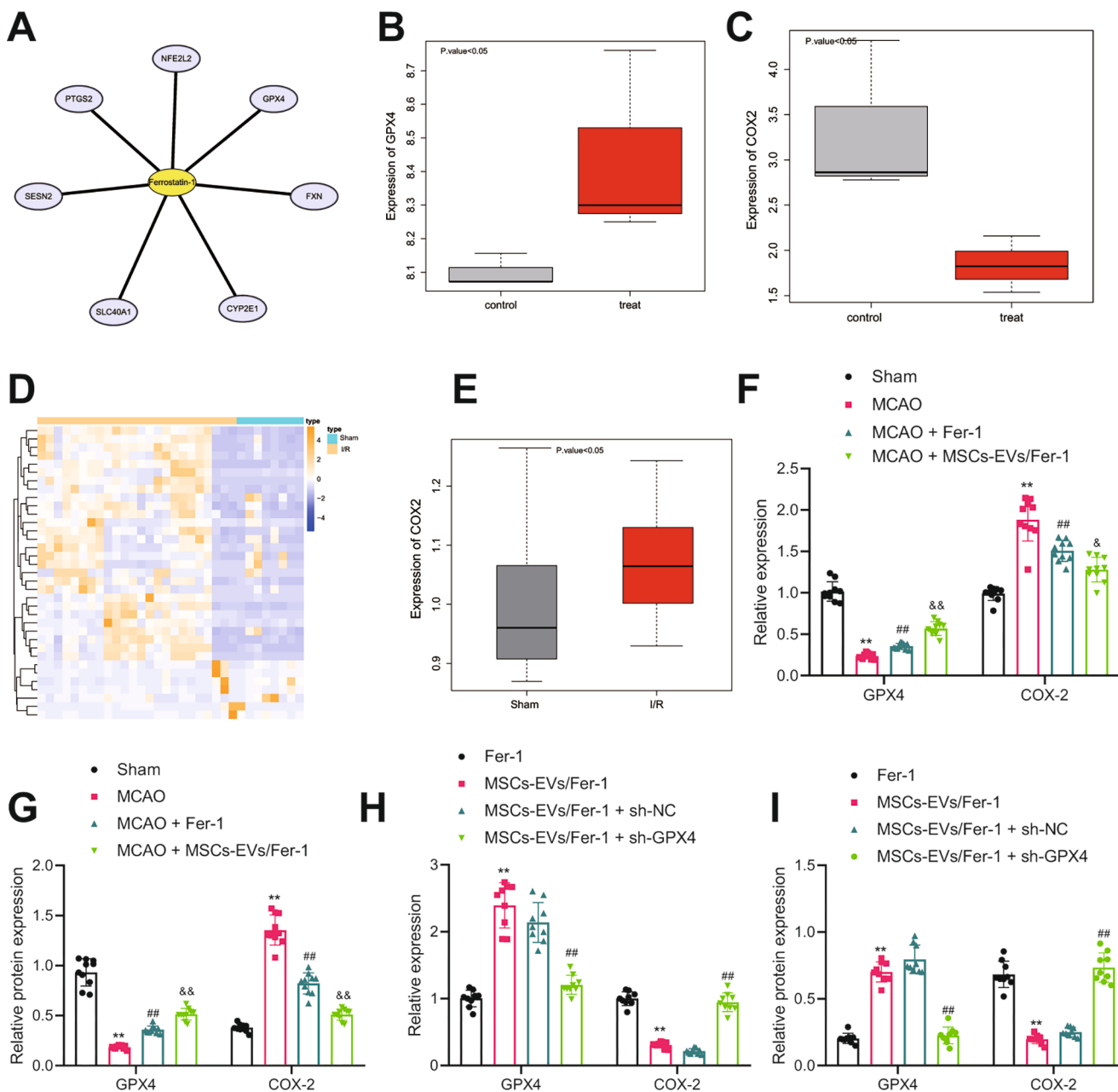


Fig. 3 Validation of MSCs-EVs/Fer-1 to regulate GPX4/COX-2 expression in hippocampal neurons *in vitro*. **A**, Map of the associated gene network of Fer-1. **B**, Expression of GPX4 in microarray GSE104462 (gray box line plot represents the control group; red box line plot represents the treatment group; n=3). **C**, Expression of COX-2 in microarray GSE104462 (gray box line plot represents the control group; red box line plot represents the treatment group; n=3). **D**, A heat map of DEGs in microarray GSE23160. **E**, Expression of COX-2 in mouse cerebral I/R-related microarray GSE23160 (gray box line plot represents the sham group, n=8; red box line plot represents I/R group, n=24). **F**, RT-qPCR detection of GPX4 and COX-2 in cerebral cortex tissues of MCAO mice in response to Fer-1 or MSCs-EVs/Fer-1. **G**,

Western blot detection of GPX4 and COX-2 proteins in the cerebral cortex tissues of MCAO mice in response to Fer-1 or MSCs-EVs/Fer-1. **H**, RT-qPCR detection of GPX4 and COX-2 expression in OGD/R-exposed hippocampal neurons in response to Fer-1 or MSCs-EVs/Fer-1. **I**, Western blot of GPX4 and COX-2 proteins in OGD/R-exposed hippocampal neurons in response to Fer-1 or MSCs-EVs/Fer-1. ** $p < 0.01$ compared with the sham group or the Fer-1 group; ## $p < 0.01$ compared with the MCAO group or the MSCs-EVs/Fer-1 + sh-NC group; & $p < 0.05$, && $p < 0.01$ compared with the MCAO+MSCs-EVs/Fer-1 group. All cell experiments were repeated 3 times

injected with Fer-1 or MSCs-EVs/Fer-1 (Fig. 2J-L). Meanwhile, inflammatory factors TNF- α , IL-1 β , and PGE2 were

upregulated in the cerebral cortex tissues of MCAO mice,

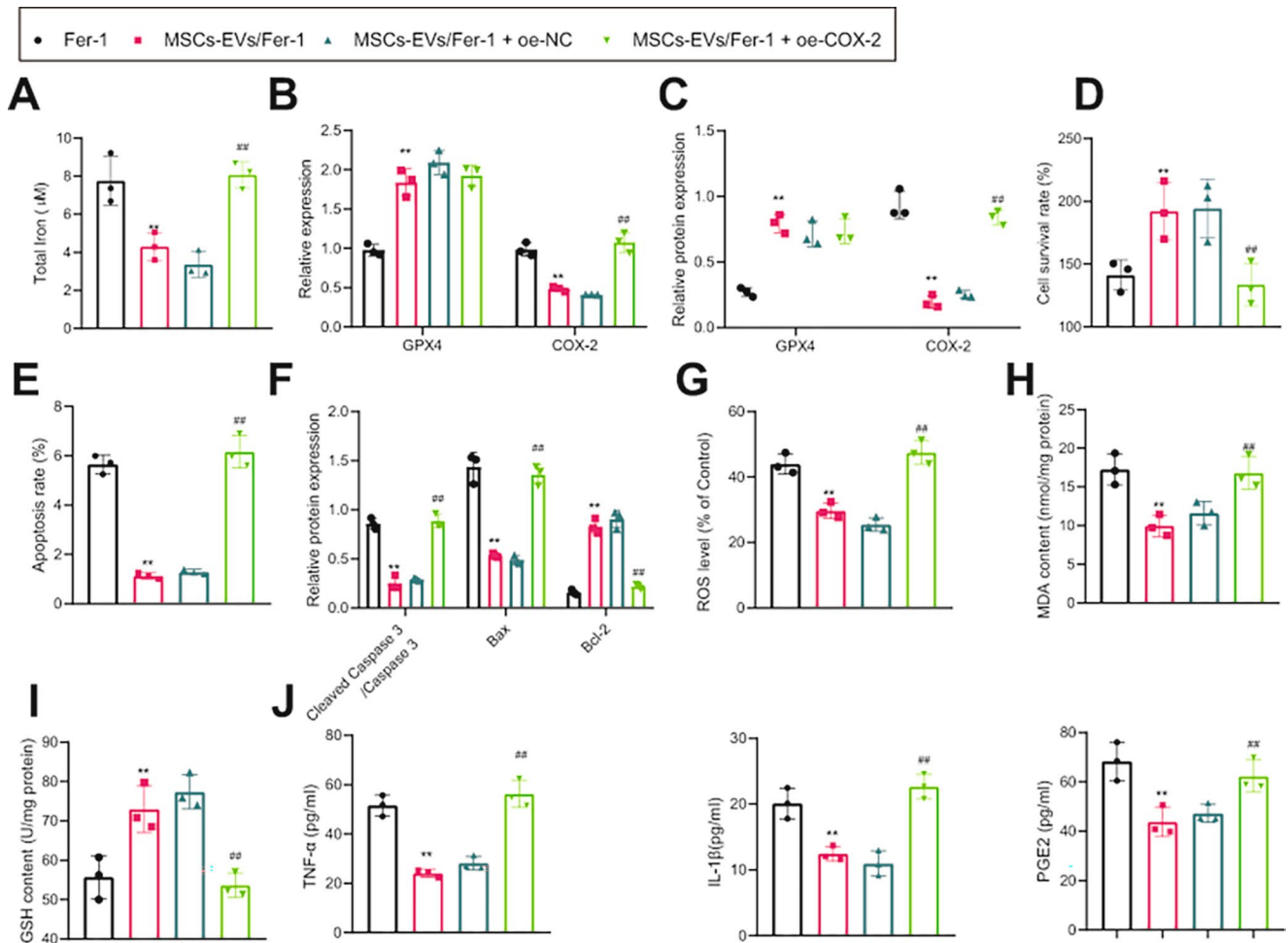


Fig. 4 Effect of MSCs-EVs/Fer-1 on OGD/R-induced hippocampal neuronal injury by modulating GPX4/COX-2 axis. **A**, Iron content in OGD/R-exposed hippocampal neurons in response to Fer-1, MSCs-EVs/Fer-1 or MSCs-EVs/Fer-1 + oe-COX-2. **B**, RT-qPCR detection of GPX4 and COX-2 mRNA expression in OGD/R-exposed hippocampal neurons in response to Fer-1, MSCs-EVs/Fer-1 or MSCs-EVs/Fer-1 + oe-COX-2. **C**, Western blot of COX-2 and GPX4 proteins in OGD/R-exposed hippocampal neurons in response to Fer-1, MSCs-EVs/Fer-1 or MSCs-EVs/Fer-1 + oe-COX-2. **D**, MTT detection of cell viability in OGD/R-exposed hippocampal neurons in response to Fer-1, MSCs-EVs/Fer-1 or MSCs-EVs/Fer-1 + oe-COX-2. **E**, Flow cytometry detection of apoptosis in OGD/R-exposed hippocampal neurons in

response to Fer-1, MSCs-EVs/Fer-1 or MSCs-EVs/Fer-1 + oe-COX-2. **F**, Western blot of apoptosis-related proteins in OGD/R-exposed hippocampal neurons in response to Fer-1, MSCs-EVs/Fer-1 or MSCs-EVs/Fer-1 + oe-COX-2. **G-I**, ROS (**G**), MDA (**H**), and GSH (**I**) production in the supernatant of OGD/R-exposed hippocampal neurons in response to Fer-1, MSCs-EVs/Fer-1 or MSCs-EVs/Fer-1 + oe-COX-2. **J**, ELISA detection of inflammatory factor levels in the supernatant of OGD/R-exposed hippocampal neurons in response to Fer-1, MSCs-EVs/Fer-1 or MSCs-EVs/Fer-1 + oe-COX-2. ** $p < 0.01$ compared with the Fer-1 group; ## $p < 0.01$ compared with the MSCs-EVs/Fer-1 + oe-NC group. All cell experiments were repeated 3 times

but downregulated in the cerebral cortex tissues of MCAO mice injected with Fer-1 or MSCs-EVs/Fer-1 (Fig. 2M).

The above results showed that MSCs-EVs loaded with Fer-1 could reduce the apoptosis of hippocampal neurons during I/R and further alleviate cerebral I/R injury by suppressing ferroptosis.

MSCs-EVs/Fer-1 Upregulate GPX4 Expression to Inhibit COX-2 Expression

To further investigate the molecular mechanism of Fer-1 protection against cerebral I/R, we obtained genes related

to the ferroptosis inhibitor Fer-1: cytochrome P4502E1 (CYP2E12), frataxin (FXN), GPX4, nuclear factor erythroid-derived 2-like 2 (NFE2L2), prostaglandin-endoperoxide synthase 2 (PTGS2), Sestrin2 (SESN2), and solute carrier family 40 member 1 (SLC40A1) through CTD database (Fig. 3A). Differential analysis of gene expression on microarray GSE104462 (before and after treatment with Fer-1) revealed that GPX4 was highly expressed after Fer-1 treatment (Fig. 3B, Supplementary Fig. 3A), while PTGS2 (alias: COX-2) was poorly expressed (Fig. 3C).

Differential expression analysis of the mouse cerebral I/R-associated microarray GSE23160 revealed that COX-2

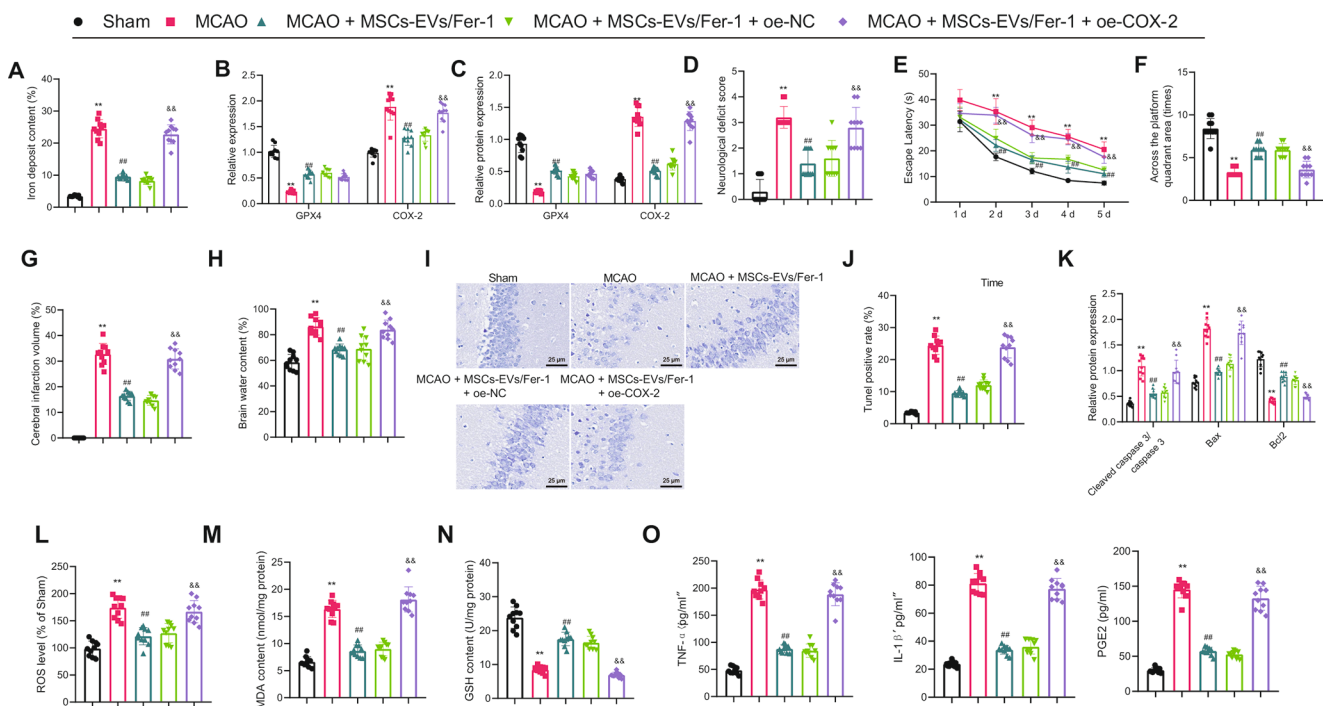


Fig. 5 Effects of MSCs-EVs/Fer-1 to regulate the GPX4/COX-2 axis on cerebral I/R injury in MCAO mice. **A**, Prussian blue staining of cerebral cortex tissues in MCAO mice in response to MSCs-EVs/Fer-1 alone or combined with oe-COX-2 (n=4). **B**, GPX4 and COX-2 mRNA expression in cerebral cortex tissues of MCAO mice in response to MSCs-EVs/Fer-1 alone or combined with oe-COX-2 determined by RT-qPCR. **C**, Western blot of COX-2 and GPX4 proteins in cerebral cortex tissues of MCAO mice in response to MSCs-EVs/Fer-1 alone or combined with oe-COX-2. **D**, Neurological deficit scores in MCAO mice in response to MSCs-EVs/Fer-1 alone or combined with oe-COX-2 (n=10). **E**, Escape latency in MCAO mice in response to MSCs-EVs/Fer-1 alone or combined with oe-COX-2. **F**, Number of times crossing the platform in MCAO mice in response to MSCs-EVs/Fer-1 alone or combined with oe-COX-2. **G**, Brain infarct area analyzed by TTC staining in MCAO mice in response to MSCs-EVs/Fer-1 alone or combined with oe-COX-2. **H**, Brain water content

detection in MCAO mice in response to MSCs-EVs/Fer-1 alone or combined with oe-COX-2. **I**, Hippocampal neuronal damage in MCAO mice in response to MSCs-EVs/Fer-1 alone or combined with oe-COX-2 determined by Nissl staining. **J**, Apoptosis of hippocampal neurons in the cerebral cortex tissues of MCAO mice in response to MSCs-EVs/Fer-1 alone or combined with oe-COX-2 determined by TUNEL staining. **K**, Western blot of apoptosis-related proteins in cerebral cortex tissues of MCAO mice in response to MSCs-EVs/Fer-1 alone or combined with oe-COX-2. **L-N**, Production of ROS (**L**), MDA (**M**), and GSH (**N**) in cerebral cortex tissues of MCAO mice in response to MSCs-EVs/Fer-1 alone or combined with oe-COX-2. **O**, ELISA detection of inflammatory factor levels in the cerebral cortex tissues of MCAO mice in response to MSCs-EVs/Fer-1 alone or combined with oe-COX-2. ** *p* < 0.01 compared with the sham group; ## *p* < 0.01 compared with MCAO group; && *p* < 0.01 compared with MSCs/EVs-Fer-1 + oe-NC group. n = 10 mice for each group

was highly expressed in I/R samples (Fig. 3D-E). Evidence has been presented demonstrating that GPX4 represses the inflammation induced by cerebral I/R in MCAO rat models by inhibiting COX-2 [22, 23]. Therefore, we selected the GPX4/COX-2 axis for further study.

GPX4 was poorly expressed, while COX-2 was highly expressed in the cerebral cortex tissues of MCAO mice, but opposite results were found in the cerebral cortex tissues of MCAO mice injected with Fer-1 or MSCs-EVs/Fer-1 (Fig. 3F-G). Moreover, consistent results for expression of GPX4 and COX-2 in hippocampal neurons were observed by reverse transcription quantitative polymerase chain reaction (RT-qPCR) and Western blot (Supplementary Fig. 3B-C).

Next, we knocked GPX4 down in hippocampal neurons in vitro while giving MSCs-EVs/Fer-1 treatment. GPX4 expression was increased while COX-2 expression

was decreased after treatment of MSCs-EVs/Fer-1 compared with the Fer-1 treatment alone. After both treatment of MSCs-EVs/Fer-1 and GPX4 silencing, GPX4 expression was decreased and COX-2 expression was increased (Fig. 3H-I).

The above results indicate that GPX4 expression was downregulated and COX-2 expression was upregulated following cerebral I/R injury, and MSCs-EVs/Fer-1 treatment in hippocampal neurons could inhibit COX-2 expression by upregulating GPX4.

MSCs-EVs/Fer-1 Protects Against OGD/R-Induced Hippocampal Neuronal Injury by Upregulating GPX4 and Inhibiting COX-2 Expression

To further investigate the effect of MSCs-EVs/Fer-1 modulation of GPX4/COX-2 axis on cerebral I/R injury, we

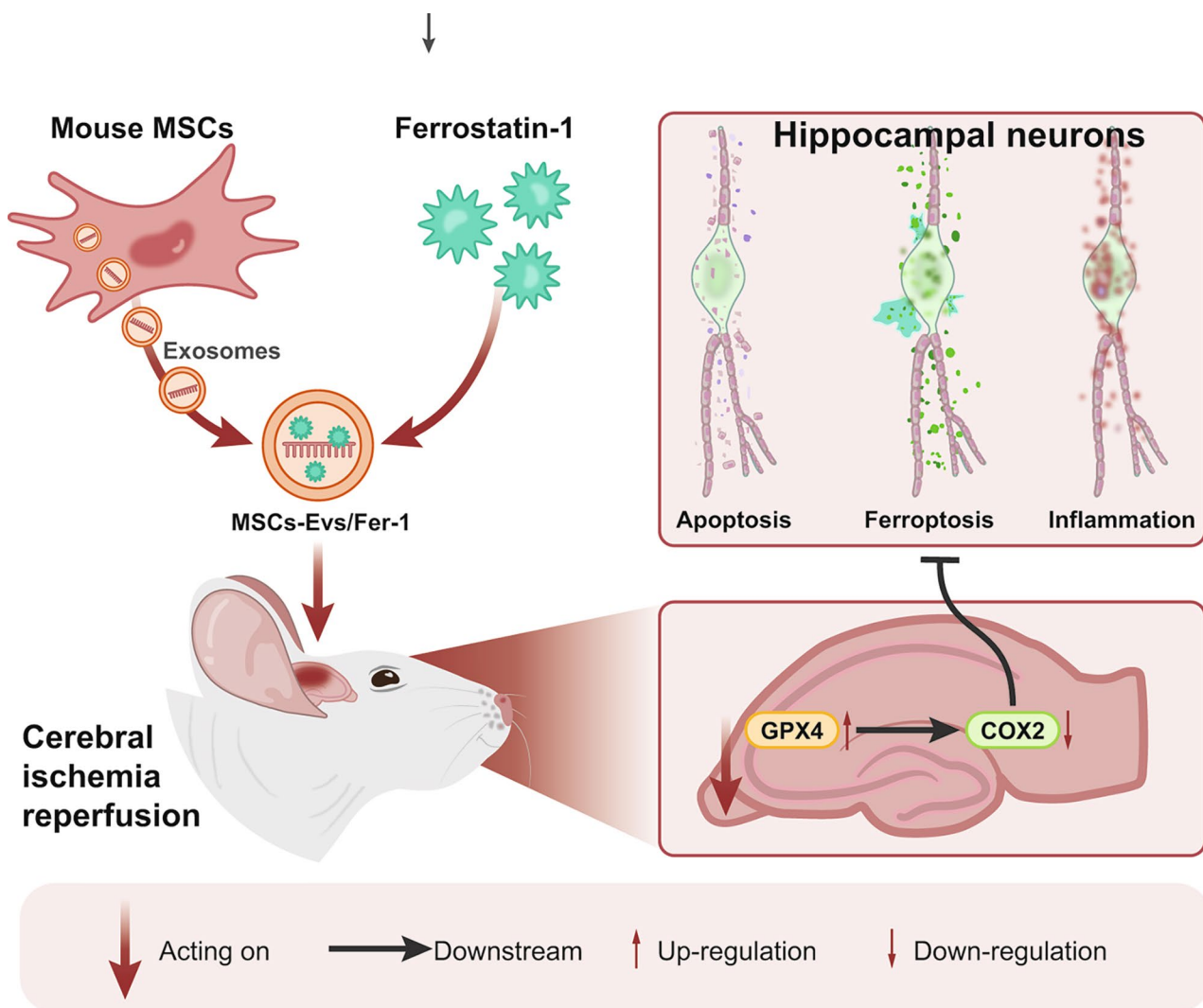


Fig. 6 Schematic illustration of the molecular mechanism by which MSCs-EVs/Fer-1 regulates the GPX4/COX-2 axis in cerebral I/R injury. MSCs-EVs/Fer-1 upregulates GPX4 expression and inhibits

COX-2 expression, which in turn inhibits ferroptosis, neuronal apoptosis and inflammation. Based on this mechanism, cerebral I/R injury was relieved by MSCs-EVs/Fer-1.

overexpressed COX-2 in OGD/R-exposed hippocampal neurons *in vitro*, accompanied with simultaneous MSCs-EVs/Fer-1 treatment. Following that, we observed accumulated iron content (Fig. 4A), increased COX-2 expression, and unchanged GPX4 expression (Fig. 4B-C).

Moreover, MSCs-EVs/Fer-1-treated OGD/R-exposed cells overexpressing COX-2 showed curtailed cell viability and enhanced apoptosis (Fig. 4D-E). Meanwhile, ratio of cleaved caspase 3/caspase 3 and Bax protein expression were promoted, while Bcl-2 protein expression was suppressed (Fig. 4F).

In the supernatant of MSCs-EVs/Fer-1-treated OGD/R-exposed cells overexpressing COX-2, production of ROS and MDA increased and that of GSH decreased (Fig. 4G-I), along with enhanced levels of inflammatory factors (Fig. 4J).

Therefore, MSCs-EVs/Fer-1 can reduce the expression of COX-2 by upregulating GPX4 expression and decreases OGD/R-induced hippocampal neuron damage.

MSCs-EVs/Fer-1 Ameliorate Cerebral I/R Injury in Mice by Upregulating GPX4 and Inhibiting COX-2 Expression

Next, we verified the effect of MSCs-EVs/Fer-1 on cerebral I/R injury in mice by regulating the GPX4/COX-2 axis. Prussian blue staining showed that iron content was reduced in the MCAO mice injected with MSCs-EVs/Fer-1, but it was then increased after COX-2 overexpression (Fig. 5A). COX-2 expression was reduced, while GPX4 expression was increased in the MCAO mice injected with MSCs-EVs/Fer-1, but further oe-COX-2 treatment increased COX-2

expression, while GPX4 expression was not significantly changed (Fig. 5B-C).

Moreover, MCAO mice injected with MSCs-EVs/Fer-1 had lower neurological scores compared with the MCAO mice, but the scores were elevated after overexpression of COX-2 (Fig. 5D). The MWM test results displayed that MCAO mice injected with MSCs-EVs/Fer-1 showed shorter escape latency and an increased number of crossing the platform. Following overexpression of COX-2, increased escape latency and decreased number of crossing the platform were observed (Fig. 5E-F). The area of cerebral infarction and the water content of cerebral cortex tissues were reduced in the MCAO mice injected MSCs-EVs/Fer-1, but then increased following overexpression of COX-2 (Fig. 5G-H).

Furthermore, hippocampal neuronal injury and apoptosis were suppressed in the cerebral cortex tissues of MCAO mice injected with MSCs-EVs/Fer-1, which were promoted by overexpressed COX-2 (Fig. 5I-J). Meanwhile, ratio of cleaved caspase 3/caspase 3 and Bax protein expression were reduced, while Bcl-2 protein expression was elevated in MCAO mice injected with MSCs-EVs/Fer-1, but overexpressed COX-2 reversed the result (Fig. 5K).

Also, ROS and MDA production was reduced in the cerebral cortex tissues of the MCAO mice injected with MSCs-EVs/Fer-1, but enhanced following overexpression of COX-2. While GSH production was elevated in the cerebral cortex tissues of the MCAO mice injected with MSCs-EVs/Fer-1, but decreased in the presence of COX-2 overexpression (Fig. 5 L-N). Meanwhile, inflammatory factors TNF- α , IL-1 β , and PGE2 were downregulated in the cerebral cortex tissues of MCAO mice injected with MSCs-EVs/Fer-1, but upregulated following overexpression of COX-2 (Fig. 5O).

Accordingly, MSCs-EVs/Fer-1 can prevent cerebral I/R injury in mice by upregulating GPX4 and suppressing COX-2 expression.

Discussion

Ferroptosis is regarded as one of the causes of reperfusion injury, which is a critical factor triggering I/R injury and even organ failure, so there is increasing attention paid on the role of ferroptosis in I/R injury-related diseases [10]. Moreover, ferroptosis can be dependent on EVs, which acts as a mutagenic mediator by transporting iron [36]. In the present study, we showed that MSCs-EVs play an essential role in controlling intracellular iron distribution by delivery of Fer-1. Meanwhile, overexpression of COX-2 could reverse the protective effects of MSCs-EVs/Fer-1 on the neuronal apoptosis *in vivo* and iron deposition *in vitro*.

We first validated that Fer-1 could be carried by MSCs-EVs. As a prior work suggested, EVs are a promising approach to control ferroptosis in targeted cells, which can be applied in different diseases and even cancers [37]. Moreover, endothelial progenitor cell-derived EVs can suppress ferroptosis of endothelial cells [38]. As the HPLC is applied to confirm drug export through EVs [39], we detected Fer-1 in EVs using HPLC and found that Fer-1 was loaded by MSCs-EVs.

After confirming that Fer-1 could be delivered to hippocampal neurons by MSCs-EVs, we further studied the role of Fer-1 in cerebral I/R injury. In the OGD/R-induced cell model, which is commonly established to simulate cerebral I/R injury [40], Fer-1 was administered to investigate ferroptosis in cerebral I/R injury. In line with our results, a previous work also reported that Fer-1 can decrease iron and even downregulate the expression of the ferroptosis-related genes [41]. Moreover, our work further showed that MSCs-EVs/Fer-1 exhibited the consistent effects as Fer-1 administration had on OGD/R-exposed cells.

We further established the MCAO mice to simulate cerebral I/R injury *in vivo*. As previously reported the overloaded intracellular iron generated a large amount of ROS through the Fenton reaction, which contributed to the ferroptosis of the cells [42]. Thus, we detected the ROS production in the cerebral cortex tissues of MCAO mice. Furthermore, 2,7-dichlorodihydrofluorescein diacetate (DCFH-DA) can enter the cells through the cell membrane and was hydrolyzed by intracellular esterase into DCFH that fails to pass through the cell membrane, and can be oxidized by ROS to produce the green fluorescent substance DCF, whose fluorescence intensity was proportional to the intracellular ROS level [43]. Therefore, DCFH-DA was used to detect the production of ROS in cerebral cortex tissues. Meanwhile, lipid peroxidation is an important initiating link for ferroptosis [44]. Inflammatory response is present throughout the pathology of cerebral I/R injury and severely affects patient prognosis [45, 46]. Based on the above, we examined the production of oxidative stress markers GSH and MDA, as well as the relevant inflammatory factors in the cortical tissues of mice. As our results shown, the administration of Fer-1 or MSCs-EVs/Fer-1 reduced ROS and MDA production, and inflammatory factor levels, but increased GSH production. These results showed that MSCs-EVs/Fer-1 inhibited ferroptosis, oxidative stress and inflammatory response.

The subsequent mechanistic investigation revealed that MSCs-EVs/Fer-1 upregulated GPX4 expression but downregulated COX-2 expression. Upregulated GPX4 expression can maintain the intracellular glutathione level to suppress ferroptosis in myocardial I/R injury [47], which is consistent with our results. Also, recovered GPX4 expression

blocked the increase of COX-2 expression [48], while inactivated COX-2 may attenuate neuronal injury and prevent cognitive deficits [49]. These existing references and our consistent results together confirmed that MSCs-EVs/Fer-1 could increase GPX4 expression but reduce COX-2 expression, therefore preventing cerebral I/R injury both *in vitro* and *in vivo*.

Conclusion

In summary, we demonstrate in this study that MSCs-EVs deliver Fer-1 into hippocampal neurons which are useful vehicles for the treatment of cerebral I/R injury. Moreover, our data indicate that MSCs-EVs/Fer-1 confer a protective role in cerebral I/R by upregulating GPX4 and inhibiting COX-2 expression, which suppresses ferroptosis in the hippocampal neurons (Fig. 6). It is of great practical significance to optimize the combined application of the MSCs-EVs/Fer-1 to assist in the establishment of a collaborative therapy that can be applied in clinical practice. However, further investigation is still required into how to obtain a large number of high-purity MSCs-EVs, how to further optimize the loading capacity of EVs, and how to realize the delivery of EVs to specific target cells.

Supplementary Information The online version contains supplementary material available at <https://doi.org/10.1007/s11064-022-03770-2>.

Acknowledgements Not applicable.

Author Contributions Junying Liu and Yamei Zhang designed the study. Yan Zhou, Chenchen Xie and Ci Li collated the data, carried out data analyses and produced the initial draft of the manuscript. Junying Liu and Li Ma contributed to drafting the manuscript. Yamei Zhang contributed to revising the manuscript. All authors have read and approved the final submitted manuscript.

Funding This work was funded by the Innovation foundation of The Affiliated Hospital of Chengdu University (CDFYCX202209), Key Project of Health Commission of Sichuan Province(18PJ030), Foundation of Affiliated Hospital of Chengdu University (YZD2017004), Project of Sichuan Education Department (17ZA0098), Research Project of Sichuan Medical Association(S21055).

Data Availability The data and materials of the study can be obtained from the corresponding author upon request.

Declarations

Conflict of Interest The authors declare no conflict of interest.

References

- Campbell BCV, Khatri P (2020) Stroke Lancet 396:129–142. [https://doi.org/10.1016/S0140-6736\(20\)31179-X](https://doi.org/10.1016/S0140-6736(20)31179-X)
- Prabhakaran S, Ruff I, Bernstein RA (2015) Acute stroke intervention: a systematic review. JAMA 313:1451–1462. <https://doi.org/10.1001/jama.2015.3058>
- Zhou L, Li F, Xu HB, Luo CX, Wu HY, Zhu MM, Lu W, Ji X, Zhou QG, Zhu DY (2010) Treatment of cerebral ischemia by disrupting ischemia-induced interaction of nNOS with PSD-95. Nat Med 16:1439–1443. <https://doi.org/10.1038/nm.2245>
- Xu F, Ma R, Zhang G, Wang S, Yin J, Wang E, Xiong E, Zhang Q, Li Y (2018) Estrogen and propofol combination therapy inhibits endoplasmic reticulum stress and remarkably attenuates cerebral ischemia-reperfusion injury and OGD injury in hippocampus. Biomed pharmacotherapy = Biomedecine pharmacotherapie 108:1596–1606. <https://doi.org/10.1016/j.biopha.2018.09.167>
- Tian X, An R, Luo Y, Li M, Xu L, Dong Z (2019) Tamibarotene Improves Hippocampus Injury Induced by Focal Cerebral Ischemia-Reperfusion via Modulating PI3K/Akt Pathway in Rats. J stroke Cerebrovasc diseases: official J Natl Stroke Association 28:1832–1840. <https://doi.org/10.1016/j.jstrokecerebrovasdis.2019.04.017>
- Tuo QZ, Liu Y, Xiang Z et al (2022) Thrombin induces ACSL4-dependent ferroptosis during cerebral ischemia/reperfusion. Signal Transduct Target therapy 7:59. <https://doi.org/10.1038/s41392-022-00917-z>
- Stockwell BR, Friedmann Angeli JP, Bayir H et al (2017) Ferroptosis: A Regulated Cell Death Nexus Linking Metabolism, Redox Biology, and Disease. Cell 171:273–285. <https://doi.org/10.1016/j.cell.2017.09.021>
- Hu Q, Zuo T, Deng L, Chen S, Yu W, Liu S, Liu J, Wang X, Fan X, Dong Z (2022) beta-Caryophyllene suppresses ferroptosis induced by cerebral ischemia reperfusion via activation of the NRF2/HO-1 signaling pathway in MCAO/R rats. Phytomedicine: Int J phytotherapy phytopharmacology 102:154112. <https://doi.org/10.1016/j.phymed.2022.154112>
- Li C, Sun G, Chen B et al (2021) Nuclear receptor coactivator 4-mediated ferritinophagy contributes to cerebral ischemia-induced ferroptosis in ischemic stroke. Pharmacol Res 174:105933. <https://doi.org/10.1016/j.phrs.2021.105933>
- Li X, Ma N, Xu J et al (2021) Targeting Ferroptosis: Pathological Mechanism and Treatment of Ischemia-Reperfusion Injury. 1587922. <https://doi.org/10.1155/2021/1587922>. Oxidative medicine and cellular longevity 2021
- Rani S, Ryan AE, Griffin MD, Ritter T (2015) Mesenchymal Stem Cell-derived Extracellular Vesicles: Toward Cell-free Therapeutic Applications. Mol therapy: J Am Soc Gene Therapy 23:812–823. <https://doi.org/10.1038/mt.2015.44>
- Qiu G, Zheng G, Ge M, Wang J, Huang R, Shu Q, Xu J (2018) Mesenchymal stem cell-derived extracellular vesicles affect disease outcomes via transfer of microRNAs. Stem Cell Res Ther 9:320. <https://doi.org/10.1186/s13287-018-1069-9>
- Zheng J, Lu T, Zhou C et al (2020) Extracellular Vesicles Derived from Human Umbilical Cord Mesenchymal Stem Cells Protect Liver Ischemia/Reperfusion Injury by Reducing CD154 Expression on CD4 + T Cells via CCT2. Adv Sci 7:1903746. <https://doi.org/10.1002/advs.201903746>
- Wang M, Yan L, Li Q, Yang Y, Turrentine M, March K, Wang IW (2022) Mesenchymal stem cell secretions improve donor heart function following ex vivo cold storage. J Thorac Cardiovasc Surg 163:e277–e292. <https://doi.org/10.1016/j.jtcvs.2020.08.095>
- Lin F, Chen W, Zhou J et al (2022) Mesenchymal stem cells protect against ferroptosis via exosome-mediated stabilization of

- SLC7A11 in acute liver injury. *Cell Death Dis* 13:271. <https://doi.org/10.1038/s41419-022-04708-w>
16. Wu L, Tian X, Zuo H, Zheng W, Li X, Yuan M, Tian X, Song H (2022) miR-124-3p delivered by exosomes from heme oxygenase-1 modified bone marrow mesenchymal stem cells inhibits ferroptosis to attenuate ischemia-reperfusion injury in steatotic grafts. *J Nanobiotechnol* 20:196. <https://doi.org/10.1186/s12951-022-01407-8>
 17. Dangol S, Chen Y, Hwang BK, Jwa NS (2019) Iron- and Reactive Oxygen Species-Dependent Ferroptotic Cell Death in Rice-Magnaporthe oryzae Interactions. *Plant Cell* 31:189–209. <https://doi.org/10.1105/tpc.18.00535>
 18. Cui Y, Zhang Z, Zhou X et al (2021) Microglia and macrophage exhibit attenuated inflammatory response and ferroptosis resistance after RSL3 stimulation via increasing Nrf2 expression. *J Neuroinflamm* 18:249. <https://doi.org/10.1186/s12974-021-02231-x>
 19. Zhao J, Wu Y, Liang S, Piao X (2022) Activation of SSAT1/ALOX15 Axis Aggravates Cerebral Ischemia/Reperfusion Injury via Triggering Neuronal Ferroptosis. *Neuroscience* 485:78–90. <https://doi.org/10.1016/j.neuroscience.2022.01.017>
 20. Kuang H, Wang T, Liu L, Tang C, Li T, Liu M, Wang T, Zhong W, Wang Y (2021) Treatment of early brain injury after subarachnoid hemorrhage in the rat model by inhibiting p53-induced ferroptosis. *Neurosci Lett* 762:136134. <https://doi.org/10.1016/j.neulet.2021.136134>
 21. Zhang J, Bi J, Ren Y et al (2021) Involvement of GPX4 in irisin's protection against ischemia reperfusion-induced acute kidney injury. *J Cell Physiol* 236:931–945. <https://doi.org/10.1002/jcp.29903>
 22. Sengupta A, Lichti UF, Carlson BA, Cataisson C, Ryscavage AO, Mikulec C, Conrad M, Fischer SM, Hatfield DL, Yuspa SH (2013) Targeted disruption of glutathione peroxidase 4 in mouse skin epithelial cells impairs postnatal hair follicle morphogenesis that is partially rescued through inhibition of COX-2. *J Invest Dermatol* 133:1731–1741. <https://doi.org/10.1038/jid.2013.52>
 23. Vaibhav K, Shrivastava P, Javed H et al (2012) Piperine suppresses cerebral ischemia-reperfusion-induced inflammation through the repression of COX-2, NOS-2, and NF-kappaB in middle cerebral artery occlusion rat model. *Mol Cell Biochem* 367:73–84. <https://doi.org/10.1007/s11010-012-1321-z>
 24. Wu X, Peng K, Huang H, Li Z, Xiang W, Deng W, Liu L, Li W, Zhang T (2019) MiR-21b-3p protects NS2OY cells against oxygen-glucose deprivation/reperfusion-induced injury by down-regulating cyclooxygenase-2. *Am J translational Res* 11:3007–3017
 25. In: th (ed) *Guide for the Care and Use of Laboratory Animals*. Washington (DC)
 26. Liao Z, Luo R, Li G, Song Y, Zhan S, Zhao K, Hua W, Zhang Y, Wu X, Yang C (2019) Exosomes from mesenchymal stem cells modulate endoplasmic reticulum stress to protect against nucleus pulposus cell death and ameliorate intervertebral disc degeneration in vivo. *Theranostics* 9:4084–4100. <https://doi.org/10.7150/thno.33638>
 27. Qin X, Guo H, Wang X et al (2019) Exosomal miR-196a derived from cancer-associated fibroblasts confers cisplatin resistance in head and neck cancer through targeting CDKN1B and ING5. *Genome Biol* 20:12. <https://doi.org/10.1186/s13059-018-1604-0>
 28. Kooijmans SAA, Stremersch S, Braeckmans K, de Smedt SC, Hendrix A, Wood MJA, Schifflers RM, Raemdonck K, Vader P (2013) Electroporation-induced siRNA precipitation obscures the efficiency of siRNA loading into extracellular vesicles. *J controlled release: official J Controlled Release Soc* 172:229–238. <https://doi.org/10.1016/j.jconrel.2013.08.014>
 29. Wang J, Li G, Tu C et al (2020) High-throughput single-cell analysis of exosome mediated dual drug delivery, in vivo fate and synergistic tumor therapy. *Nanoscale* 12:13742–13756. <https://doi.org/10.1039/d0nr02344b>
 30. He Q, Li Z, Meng C, Wu J, Zhao Y, Zhao J (2019) Parkin-Dependent Mitophagy is Required for the Inhibition of ATF4 on NLRP3 Inflammasome Activation in Cerebral Ischemia-Reperfusion Injury in Rats. *Cells* 8. <https://doi.org/10.3390/cells8080897>
 31. Fu D, Wang C, Yu L et al (2021) Induction of ferroptosis by ATF3 elevation alleviates cisplatin resistance in gastric cancer by restraining Nrf2/Keap1/xCT signaling. *Cell Mol Biol Lett* 26:26. <https://doi.org/10.1186/s11658-021-00271-y>
 32. Li L, Yang L, Yang F et al (2021) Ginkgo biloba Extract 50 (GBE50) Ameliorates Insulin Resistance, Hepatic Steatosis and Liver Injury in High Fat Diet-Fed Mice. *J Inflamm Res* 14:1959–1971. <https://doi.org/10.2147/JIR.S302934>
 33. Li S, Zhao X, Lazarovici P, Zheng W (2019) Artemether Activation of AMPK/GSK3beta(ser9)/Nrf2 Signaling Confers Neuroprotection towards beta-Amyloid-Induced Neurotoxicity in 3xTg Alzheimer's Mouse Model. *Oxidative Med Cell Longev* 2019:1862437. <https://doi.org/10.1155/2019/1862437>
 34. Li S, Peng T, Zhao X, Silva M, Liu L, Zhou W, Chen L, Zheng W (2021) Artemether confers neuroprotection on cerebral ischemic injury through stimulation of the Erk1/2-P90rsk-CREB signaling pathway. *Redox Biol* 46:102069. <https://doi.org/10.1016/j.redox.2021.102069>
 35. Luo L, Zang G, Liu B, Qin X, Zhang Y, Chen Y, Zhang H, Wu W, Wang G (2021) Bioengineering CXCR4-overexpressing cell membrane functionalized ROS-responsive nanotherapeutics for targeting cerebral ischemia-reperfusion injury. *Theranostics* 11:8043–8056. <https://doi.org/10.7150/thno.60785>
 36. Ito F, Kato K, Yanatori I, Murohara T, Toyokuni S (2021) Ferroptosis-dependent extracellular vesicles from macrophage contribute to asbestos-induced mesothelial carcinogenesis through loading ferritin. *Redox Biol* 47:102174. <https://doi.org/10.1016/j.redox.2021.102174>
 37. Wu S, Li T, Liu W, Huang Y (2021) Ferroptosis and Cancer: Complex Relationship and Potential Application of Exosomes. *Front cell Dev biology* 9:733751. <https://doi.org/10.3389/fcell.2021.733751>
 38. Li L, Wang H, Zhang J, Chen X, Zhang Z, Li Q (2021) Effect of endothelial progenitor cell-derived extracellular vesicles on endothelial cell ferroptosis and atherosclerotic vascular endothelial injury. *Cell death discovery* 7:235. <https://doi.org/10.1038/s41420-021-00610-0>
 39. Hekmatirad S, Moloudizargari M, Moghadamnia AA, Kazemi S, Mohammadnia-Afrouzi M, Baeceri M, Moradkhani F, Asghari MH (2021) Inhibition of Exosome Release Sensitizes U937 Cells to PEGylated Liposomal Doxorubicin. *Front Immunol* 12:692654. <https://doi.org/10.3389/fimmu.2021.692654>
 40. Wang L, Tan Y, Zhu Z, Chen J, Sun Q, Ai Z, Ai C, Xing Y, He G, Liu Y (2021) ATP2B1-AS1 Promotes Cerebral Ischemia/Reperfusion Injury Through Regulating the miR-330-5p/TLR4-MyD88-NF-kappaB Signaling Pathway. *Front cell Dev biology* 9:720468. <https://doi.org/10.3389/fcell.2021.720468>
 41. Ge H, Xue X, Xian J et al (2022) Ferostatin-1 Alleviates White Matter Injury Via Decreasing Ferroptosis Following Spinal Cord Injury. *Mol Neurobiol* 59:161–176. <https://doi.org/10.1007/s12035-021-02571-y>
 42. Yang WS, Stockwell BR (2016) Ferroptosis: Death by Lipid Peroxidation. *Trends Cell Biol* 26:165–176. <https://doi.org/10.1016/j.tcb.2015.10.014>
 43. Zhu Y, Ruan S, Shen H, Guan Q, Zhai L, Yang Y (2021) Oridonin regulates the polarized state of Kupffer cells to alleviate nonalcoholic fatty liver disease through ROS-NF-kappaB. *Int Immunopharmacol* 101:108290. <https://doi.org/10.1016/j.intimp.2021.108290>

44. Sang M, Luo R, Bai Y, Dou J, Zhang Z, Liu F, Feng F, Xu J, Liu W (2019) Mitochondrial membrane anchored photosensitive nano-device for lipid hydroperoxides burst and inducing ferroptosis to surmount therapy-resistant cancer. *Theranostics* 9:6209–6223. <https://doi.org/10.7150/thno.36283>
45. Acosta SA, Tajiri N, Hoover J, Kaneko Y, Borlongan CV (2015) Intravenous Bone Marrow Stem Cell Grafts Preferentially Migrate to Spleen and Abrogate Chronic Inflammation in Stroke. *Stroke* 46:2616–2627. <https://doi.org/10.1161/STROKEAHA.115.009854>
46. Dabrowska S, Andrzejewska A, Strzemecki D, Muraca M, Janowski M, Lukomska B (2019) Human bone marrow mesenchymal stem cell-derived extracellular vesicles attenuate neuroinflammation evoked by focal brain injury in rats. *J Neuroinflamm* 16:216. <https://doi.org/10.1186/s12974-019-1602-5>
47. Hwang JW, Park JH, Park BW et al (2021) Histochole Attenuates Myocardial Ischemia-Reperfusion Injury by Inhibiting Ferroptosis-Induced Cardiomyocyte Death. <https://doi.org/10.3390/antiox10101624>. *Antioxidants* 10
48. Peng W, Zhu Z, Yang Y, Hou J, Lu J, Chen C, Liu F, Pi R (2021) N2L, a novel lipoic acid-niacin dimer, attenuates ferroptosis and decreases lipid peroxidation in HT22 cells. *Brain Res Bull* 174:250–259. <https://doi.org/10.1016/j.brainresbull.2021.06.014>
49. Zhu X, Yao Y, Yang J, Zhengxie J, Li X, Hu S, Zhang A, Dong J, Zhang C, Gan G (2020) COX-2-PGE2 signaling pathway contributes to hippocampal neuronal injury and cognitive impairment in PTZ-kindled epilepsy mice. *Int Immunopharmacol* 87:106801. <https://doi.org/10.1016/j.intimp.2020.106801>

Publisher's Note Springer Nature remains neutral with regard to jurisdictional claims in published maps and institutional affiliations.

Springer Nature or its licensor holds exclusive rights to this article under a publishing agreement with the author(s) or other rightsholder(s); author self-archiving of the accepted manuscript version of this article is solely governed by the terms of such publishing agreement and applicable law.